AIAA JOURNAL
Vol. 40, No. 4, April 2002

# Tail Buffet Alleviation of High-Performance Twin-Tail Aircraft Using Piezostack Actuators

S. Hanagud,* M. Bayon de Noyer,† and H. Luo‡
*Georgia Institute of Technology, Atlanta, Georgia 30332-0150*
D. Henderson§
*U.S. Air Force Research Laboratory, Wright–Patterson Air Force Base, Ohio 45433*
and
K. S. Nagaraja¶
*Rohini International, Beavercreek, Ohio 45434*

**The phenomenon of the tail buffet is usually associated with high-angle-of-attack operations of a twin-tail aircraft. The unsteady pressures that result from the tail buffet, along with the aeroelastic coupling of the vertical tail structural assembly, cause vibrations of the empennage structural assembly. Such buffet-induced vibrations can shorten the fatigue life the empennage structure and limit the flight envelope of the aircraft due to the large amplitudes of the fin vibrations. Methods of alleviating the tail buffet-induced vibrations, by the use of smart structure concepts, is presented. Theoretical and experimental investigations were conducted to estimate and enhance the required control authority for tail buffet alleviation using piezoceramic-stack-based actuators. This was accomplished by designing an effective piezoelectric ceramic actuator assembly, developing procedures to place the sensors and actuators optimally on the vertical tail subassembly, designing controllers using acceleration feedback control concepts, and developing procedures to implement these controllers by using digital signal processor-based systems. The effectiveness of multimode controllers was validated by testing a full-scale laboratory subassembly under excitation provided by a shaker and wind-tunnel tests on a $\frac{1}{16}$th-scale model with aeroelastically tailored vertical tail subassembly.**

## Nomenclature

| | | |
|---|---|---|
| $A$, $B$ | = | corresponding state-space matrices |
| $A_{il}$ | = | combination of the modal amplitude, sensor influence, and actuator influence functions |
| $a_1$, $a_2$ | = | actuator and sensor location parameter |
| $E_{33}$, $d_{33}$ | = | longitudinal short-circuit Young's modulus and longitudinal piezoelectric charge constant of the piezoceramic element |
| $F_b$ | = | blocked force of the stack |
| $f(t)$ | = | buffet load |
| $f_k(t)$ | = | excitation force at point $k$ |
| $f_k$ | = | Laplace transform of $f_k(t)$ |
| $G_{ci}$ | = | controller driving the $i$th actuator array: transfer function between the input voltage to the $i$th actuator array $u_i(t)$ and voltage from the control sensor $y_s(t)$ |
| $G_{pk}$ | = | open-loop transfer function between performance sensor and excitation force |
| $G_{pui}$ | = | open-loop transfer function between performance sensor and input voltage and $i$th actuator array |
| $G_{sk}$ | = | open-loop transfer function between control sensor and excitation force |
| $G_{sui}$ | = | open-loop transfer function between control sensor and input voltage and $i$th actuator array |
| $L$, $t$, $w$, $n$ | = | length, thickness, and width of the piezoceramic element, and number of piezoceramic elements of the stack, respectively |
| $M$, $C$, $K$ | = | mass, damping, and stiffness matrices of the system |
| $u_i(t)$ | = | input voltage of actuator array |
| $V$ | = | voltage applied across the actuator |
| $y_p(t)$ | = | performance sensor response located at point $p$ |
| $\bar{y}_p$ | = | Laplace transform of $y_p(t)$ |
| $y_s(t)$ | = | voltage from control sensor |
| $\gamma_{cil}$ | = | scalar gain of controller (for the control of the $l$th mode with the $i$th actuator array) |
| $\Delta L$ | = | free elongation of the stack |
| $\zeta_{cil}$ | = | damping ratio of compensator (for the control of the $l$th mode with the $i$th actuator array) |
| $\zeta_i$ | = | damping ratio of the $i$th mode |
| $\zeta_{il}$ | = | damping ratio of structure (for the control of the $l$th mode with the $i$th actuator array) |
| $\eta$ | = | modal space coordinates of controller |
| $\xi$, $X$, $x$, $\bar{x}$ | = | modal space, state space, configuration space, and Laplace transform coordinates of the system |
| $\omega_{cil}$ | = | natural frequency of compensator (for control of the $l$th mode with the $i$th actuator array) |
| $\omega_i$ | = | natural frequency of the $i$th mode |
| $\omega_{il}$ | = | natural frequency of structure (for control of the $l$th mode with the $i$th actuator array) |
| $\omega_s$, $\omega_c$ | = | natural frequency of system and controller |

Received 12 May 2000; revision received 15 February 2001; accepted for publication 9 April 2001. 

*Professor, School of Aerospace Engineering. Associate Fellow AIAA.
†Ph.D. Student, School of Aerospace Engineering.
‡Postdoctoral Fellow, School of Aerospace Engineering; currently Staff Engineer, Engineering Mechanics Laboratory, General Electric Global Research Center, K1 4B36, One Research Circle, Niskayuna, NY 12309.
§Aerospace Engineer, Control Systems Development and Application Branch, Air Vehicle Directorate. Member AIAA.
¶President, 3354 South Field Drive.

## Introduction

IN high-performance twin-tail aircraft (HPTTA), tail buffet was first noticed through its destructive effects of induced fatigue cracks.[1] During high-angle-of-attack maneuvers, vortices are generated at different locations such as the wing–fuselage interface and the leading-edge extensions. The vortices can breakup and create a separated flow. The separated flow is convected, by the geometry of the wing–fuselage interface, toward the twin vertical tails (Fig. 1).

**Fig. 1 Typical buffet in a twin-tail aircraft.**

The unsteady pressures, associated with the separated flow, excite the vibration modes of the vertical fin structural assemblies. This, along with the aeroelastic coupling of the tail structural assembly, results in vibrations that can shorten the fatigue life of the empennage assembly and limit the flight envelope of the aircraft due to the large amplitude of the fin vibrations.

The set of HPTTA includes the F-14, F-15, F/A-18, and F-22. Because the characteristic of the separated flow depends on the geometry of the wing, the fuselage, and the empennage, different kinds of tail buffet exist. A typical buffet in a twin-tail aircraft is shown in Fig. 1. Vibrations of the vertical tails of the F/A-18 are attributed to broadband excitations, resulting from the bursting of strong vortices.[2] On the other hand, the tail buffet problem of the F-15 is associated with a separated flow containing a narrow band of frequencies that engulfs the tail assembly.[3] This narrow band of frequencies contains the frequency of the first torsion mode of the vertical tails.

## Tail Buffet Alleviation

Many different approaches to tail buffet alleviation have been investigated. Some of the approaches, such as the wing leading-edge blowing[4–21] or adding fences[6–10] on the wings or on the fuselage, are related to flow control. Other approaches that address the problems are through passive structural design modifications. An example of this approach is the reinforcement of the fin assembly with a composite patch,[1] both to repair existing defects and to stiffen the assembly. More recently, active structural control techniques have been investigated. A combination of feedback controllers and the use of the rudders were first evaluated.[21–23] Currently, techniques based on smart structure concepts, which use active structural actuators, such as piezoceramic wafers[23–27] and different types of controllers, are being investigated.

## Outline

The objective of this paper is to describe the results of our work in the area of buffet alleviation, by the use of piezoelectric ceramic (piezoceramic) stack actuator assemblies, in combination with acceleration feedback control. This is accomplished by, first, obtaining a mathematical model for the vertical tail subassembly without control. The subsequent steps are to select the sensors, select the actuators, and design the actuator assemblies to maximize the control authority. Once the actuator assembly is designed, further optimization of the control authority is achieved through an optimal placement of the sensors and actuators. This step is followed by the design of controllers, by using acceleration feedback control concepts. At this stage, the closed-loop system consisted of the structural assembly to be controlled, bonded actuator assemblies and sensors at optimal locations, and controllers that are implemented through a digital signal processor-based system.

The designed vibration controllers were first tested on a full-scale vertical tail subassembly to validate the multimode control capability in the frequency range of 8–80 Hz. Then, $\frac{1}{16}$th-scale wind-tunnel models of a selected HPTTA, with aeroelastically scaled empennage, were designed and built. The buffet control of these models was tested, in a wind tunnel, at angles of attack ranging from 0 to 23 deg. The first series of wind-tunnel tests were to obtain information on buffet loads and to estimate the needed control authority to reduce the peak buffet-induced dynamic response of the vertical tail at least by a factor of 5. Information from the first series of tests was used to design the parameters of the piezoceramic stack actuator assemblies that can reduce the peak dynamic response at least by a factor of 5. The next series of wind-tunnel tests were conducted to validate high-authority piezoceramic-stack-based actuator assemblies and the associated control system in controlling buffet-induced vibration.

## Models for Controller Designs

Depending on the procedure used for the design of the controllers, the plant model (the structural dynamic model) of a given structure can be one of the following: a finite element model in the configuration space,

$$M\ddot{x} + C\dot{x} + Kx = f \tag{1}$$

a finite element model in the modal space,

$$\ddot{\xi} + \mathrm{diag}(2\zeta_i w_i)\dot{\xi} + \mathrm{diag}\left(w_i^2\right)\xi = F \tag{2}$$

a finite element model in the state space,

$$\dot{X} = AX + Bu \tag{3}$$

or a transfer function matrix model,

$$\bar{x} = [TF]\bar{f} = (s^2M + sC + K)^{-1}\bar{f} \tag{4}$$

These models were obtained as follows.

A full-scale laboratory vertical tail subassembly of the selected HPTTA was available in the School of Aerospace Engineering at Georgia Institute of Technology. This vertical tail subassembly consisted of one vertical tail, one horizontal tail, and a part of the aft-fuselage. The subassembly was mounted on a specially designed framework and supports. These supports were designed such that the dominant natural frequencies and mode shapes of the laboratory subassembly (see Figs. 2 and 3) were nearly the same as those obtained during the full-scale aircraft tests.

A detailed experimental modal analysis of the laboratory vertical tail subassembly was performed. During this test, a 111.2-N (25-lbf) shaker was attached to the outboard trailing edge of the tip of the vertical tail, and 41 sensor locations were selected for the vertical tail. In addition, nine locations were also selected on the horizontal tail.

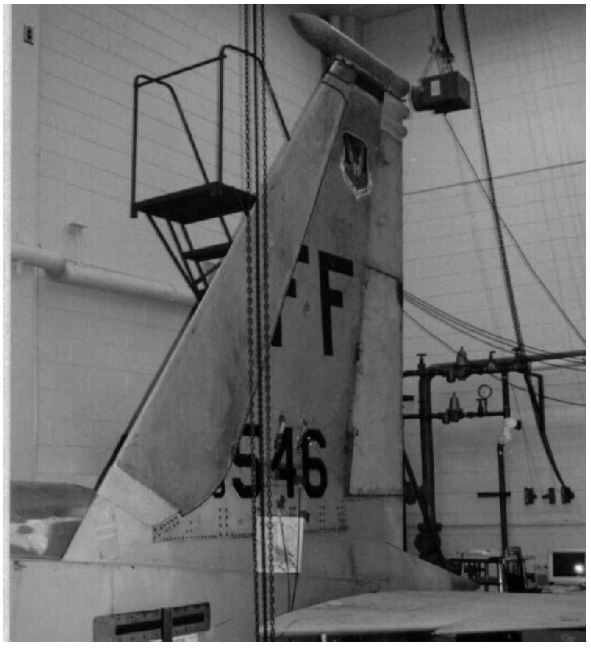

**Fig. 2 Laboratory vertical tail subassembly.**

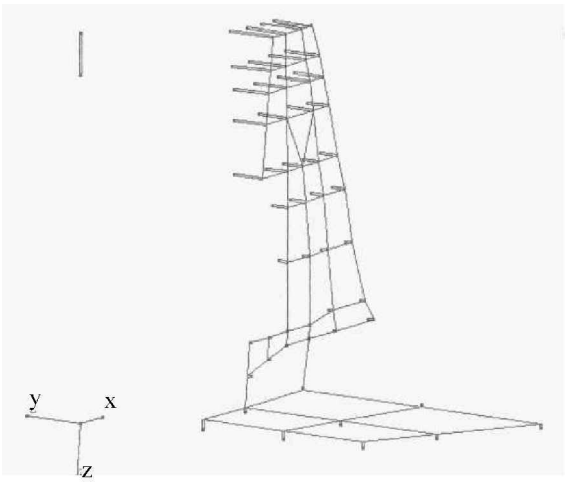


**Fig. 3 Mode shape of the first bending mode of the laboratory vertical tail subassembly.**

From this experiment, a new model for the vertical tail subassembly was obtained in the form of a transfer function matrix yielding the natural frequencies, the mode shapes, and the damping ratios of the system. The first 14 modes of the structure were obtained, and a $14 \times 41$ mode shape matrix was computed. With the use of the mass data from an available NASTRAN finite element model of the selected HPTTA and the reduction to the 41 experimental nodal coordinates, stiffness and damping matrices were identified. As a result, we obtained three types of models, similar to Eqs. (1), (2), and (4), from the experimental data and the available NASTRAN finite element mass matrix and identification techniques. These models are used in the design of the active vibration controller.

## Actuator and Actuator-Assembly Choice: Piezostack Actuators

In the control of buffet-induced vibrations, by using smart structures concepts, the primary concern is the control authority that can be generated by the actuator. To obtain a maximum control authority, the resultant forces that the actuator develops should be as large as possible. The control authority of piezoelectric transducer (PZT) wafer actuators, unless used in large quantities, is usually not sufficient.[23–26] In addition, in an environment of large-amplitude vibrations, PZT wafers could fracture due to their brittleness. Piezoceramic stack actuators, however, can increase the control authority through a more efficient use of the piezoceramic material properties. This increase is obtained by the use of the longitudinal $d_{33}$ coefficient instead of the transverse $d_{31}$ and $d_{32}$ coefficients generally used with wafers. The increased stack forces result from the addition of the effective piezoelectric reactions by using the accumulation of reaction from each PZT in series and the design of the actuator subassembly, as shown in Fig. 4. The free elongation $\Delta L$ and blocked force $F_b$ are

$$\Delta L = nd_{33}V \tag{5}$$

$$F_b = nd_{33}VE_{33}hw/L \tag{6}$$

The main challenge, associated with the use of the piezoceramic stack, is that the stack produces only longitudinal motion or forces. An assembly must be designed to transform the longitudinal motion of the stack into moments that will produce the control actuation. Such a transformation can be achieved by placing the piezoceramic stack parallel to the controlled structure at a distance from its neutral axis and at a selected orientation to create local moments on the structure.

The added requirement that the active element, the piezoceramic stack, must be removable while the mount is attached to the structure results in a design shown in Fig. 4. The design consists of a piezoelectric ceramic stack clamped between two blocks that are attached to the host structure. In this design, the need, for rounded point contact between the stack and the mounts, is due to the low strength of the piezoceramic stack in bending. A bolt is used both to facilitate the removal of the piezostack and to precompress the active element mechanically.

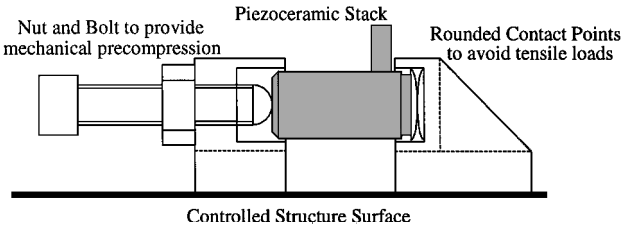


**Fig. 4 Actuator assembly.**

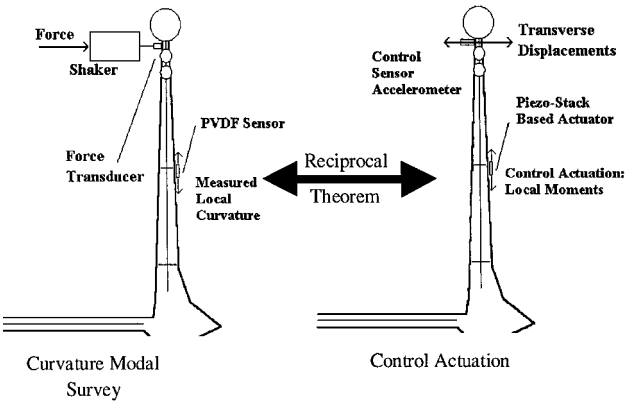


**Fig. 5 Principles of curvature modal survey.**

## Sensor and Actuator Placement: Curvature Modal Survey Approach

The second major task, in optimizing the control authority, is the placement of the sensors and actuator arrays. An actuator array is a series of actuators that will be driven by the same control signal. Depending on the types of mode to be controlled, single or multiple actuator arrays may be needed. Locations of accelerometer sensors should be chosen so that all modes in the control range are sensed. These modes include both controlled and uncontrolled modes. Furthermore, the sensor is placed such that its signal-to-noise ratio is maximum. To obtain the sensor location, the results of a classical (displacement) modal survey of the system to be controlled are used. Then, the modes are weighted and superposed to account for their importance. The location with maximum added modal response is then chosen as the sensor location.

The initial choices for the placement of the actuator arrays result directly from the types of modes to be controlled and the displacement modal survey. The actuator locations are optimized by performing a local curvature modal survey. The principles of this survey are based on the reciprocity theory as shown in Fig. 5. The optimization is performed such that local moment acting on the structure resulting from the piezostack actuator assembly produces maximum transverse motion at the sensor location. Using the reciprocity theory, the curvature modal survey is performed by exciting transversally the structure at the sensor location and measuring the response from a polyvinyldene fluoride (PVDF) sensor around the candidate actuator locations. The PVDF sensor is a piezoelectric polymer-based sensor that can be used measure the curvatures.[28] This survey is performed in all three directions so that the actuator locations are optimized for all modes that were selected for active control.

## Controller Design: Acceleration Feedback Control Compensators

The objective is to design controllers that can reduce the amplitude of vibration in a selected frequency range (8–80 Hz for the selected HPTTA). One way of achieving this objective is to provide an additional amount of selected amount of damping in the closed loop by using active control techniques.

Previous investigations, in the field of buffet alleviation, have used different types of controllers such as neural predictive controller, linear quadratic Gaussian (LQG), proportional integral derivative

(PID), frequency-domain compensation, and direct feedback. Each controller has some advantages and some drawbacks. In this work, the selected controller is the acceleration feedback controller with actuators placed at optimal locations. Reasons for selecting the acceleration feedback control are as follows. The acceleration feedback controller has a relative degree of two between the denominator and the numerator of the controller transfer function. Thus, the magnitude of the transfer function decreases rapidly as the frequency increases. Then, the rolloff, at high frequencies, is 40 dB/decade. The phase at these frequencies is 0 or 180 deg. The fast rolloff avoids any interaction with unmodeled higher-order modes in the plant model. The phase angle is beneficial for designing the system with noncollocated sensors and actuators. The acceleration feedback controllers also result in second-order controllers that are easy to implement digitally.

To control the flexible structures, system equations are usually rewritten in a state-space domain. However, these transformations to state-space domain often lose insight into the physics of the problem from the point of view of a structural dynamicist. Since the work of Goh and Caughey[29] and the introduction of the positive position feedback (PPF) controller, which was later experimentally applied to structures using piezoceramic actuators, the second-order compensators enable designers to keep the system equations of motion in their second-order form. However, this control scheme is not unconditionally stable. A second-order compensator using acceleration feedback was later developed.[30–31] The main advantage of this control scheme was its unconditional stability for single-degree-of-freedom systems with collocated pairs of sensors and actuators. Goh and Yan[32] developed a method for assigning the damping ratios and scalar gains of the compensators using pairs of collocated sensors and actuators.

Bayon de Noyer and Hanagud[33] have shown that the acceleration feedback control can also be applied to noncollocated actuators and sensors. The application for buffet-induced vibration control requires noncollocated sensors and actuators. Two methods[34] have been developed to obtain the parameters of the compensators for both single-mode and multimode control using a single actuator or a single actuator array and a noncollocated sensor. One of the methods is based on a crossover point design, and the second method is based on the $H_2$ optimization of the closed-loop transfer function. Bayon de Noyer and Hanagud[33] have also shown that a multimode controller design, for a coupled controlled dynamic system, can be reduced in the modal space into a subset of single-degree-offreedom uncoupled acceleration feedback controlled modes and a subset of uncontrolled and uncoupled structural vibration modes. As a result, each compensator can be designed independently using a selective singele-degree-of-freedom design.

**Controller Design**

Principles of the acceleration feedback controller (AFC) and the role of the offset piezoceramic actuator assembly (OPSA) in AFC can be explained by considering a one-degree-of-freedom structural dynamic system:

$$\ddot{\xi} + 2\zeta_s\omega_s\dot{\xi} + \omega_s^2\xi = a_1\gamma\omega_c^2\ddot{\eta} + f \tag{7a}$$

$$\ddot{\eta} + 2\zeta_c\omega_c\dot{\eta} + \omega_c^2\eta = a_2\ddot{\xi} \tag{7b}$$

The left-hand side of Eq. (7a) is the structural system, with $\xi$ as the displacement. The buffet load is represented by $f(t)$. Similarly, the left-hand side of Eq. (7b) is the controller, and the controller system is an electronic system and resides in the computer and the digital signal processing system. The solution $\eta(t)$ is obtained, corresponding to the sensor input $\ddot{\xi}(t)$ and the sensor location parameter $a_2$. This solution determines the control force, which is the first term on the right-hand side of the Eq. (7a). (Other quantities in this term are the actuator location parameter $a_1$ and the controller gain $\gamma$.) This control force, however, is implemented by the actuator OPSA. The design of OPSA, including the selected piezoceramic stack characteristics, the offset, and the maximum voltage, limits the maximum control force and, hence, the control authority that is achievable. Because accurate procedures for the quantitative estimation of the buffet loads are not available, OPSA design parameters were estimated by conducting preliminary closed-loop wind-tunnel tests with PZT wafer actuators.

For buffet alleviation of the HPTTA, a different controller is designed for each actuator array. Furthermore, each controller is designed by implementing in parallel single-degree-of-freedom compensators that will control each mode individually. The single-degree-of-freedom compensators can be designed following either the crossover point approach or the $H_2$ optimization of the closed-loop transfer function approach. Regardless of the choice of the approach, a single design parameter has to be set. For our purposes, the damping of each compensator is set to a number $\alpha$ times the open-loop value of the damping ratio of the mode it will suppress. Each $\alpha$ is chosen such that maximum efficiency of the controller is obtained without exceeding the maximum voltage allowable for the actuators. For the crossover point design, to the control of the $l$th mode with the $i$th actuator array, the compensator parameter design equations are[33]

$$\omega_{cil} = \omega_{il} \tag{8a}$$

$$\zeta_{cil} = \alpha_{il}\zeta_{il} \tag{8b}$$

$$\gamma_{cil} = (\zeta_{cil} - \zeta_{il})^2 \big/ A_{il} \tag{8c}$$

The $H_2$ optimization of the closed-loop transfer function to the control of the $l$th mode with the $i$th actuator array yields the following equations to design[34]:

$$\omega_{cil} = \omega_{il} \tag{9a}$$

$$\zeta_{cil} = \alpha_{il}\zeta_{il} \tag{9b}$$

$$\gamma_{cil} = 4\left(\zeta_{cil}^2 \big/ A_{il}\right) \tag{9c}$$

Note that the $H_2$ optimization of the closed-loop transfer function is not the standard LQG controller because the control effort weighting matrix is singular. This design, for the acceleration feedback controller, results from the minimization of the $H_2$ norm of the closed-loop impulse response, which is also the minimization of the closed-loop covariance of the displacement in the presence of unit white noise disturbance (M. Bayon de Noyer and S. Hanagud, "Closed-Loop Displacement Response Minimization Design for Acceleration Feedback Control," to be published). The optimum controllers were designed in the frequency domain and state-space domain. Both approaches yield the same design parameters (Bayon de Noyer and Hanagud, to be published).

**Stability Assessment**

The controller driving the $i$th actuator array is given by the transfer function between the input voltage to that actuator array $u_i(t)$ and the voltage from the control sensor $y_s(t)$ (Ref. 33):

$$G_{ci} = \frac{\bar{u}_i}{\bar{y}_s}(j\omega) = \sum_l \frac{-\gamma_{cil}\omega_{cil}^2}{-\omega^2 + 2\zeta_{cil}\omega_{cil}j\omega + \omega_{cil}^2} \tag{10}$$

In this paper, all control schemes are single-input/multi-output (SIMO) controllers. It is assumed that there are two types of sensors. The first type is the control sensor that is located such that all modes of interest are observed. The second type of sensor is the performance sensor. This sensor is located in a position where the reduction in vibration is measured. The location is selected such that a reduction of vibration amplitudes at this location is a measure of the global reduction of vibration amplitude. First, a performance sensor response $y_p(t)$ located at point $p$ and an excitation force $f_k(t)$ driving the system at point $k$ is considered. For a SIMO control scheme, the closed-loop transfer function between $y_p$ and $f_k$ is given by

$$\left.\frac{\bar{y}_p}{\bar{f}_k}\right|_{cl} = \frac{G_{pk} + \sum_i G_{ci}(G_{pui}G_{sk} - G_{sui}G_{pk})}{1 - \sum_i G_{ci}G_{sui}} \tag{11}$$

A sufficient condition for the stability of the closed-loop system is that the poles of the closed-loop transfer function between $y_p$ and $f_k$ have negative real parts for any performance sensor and disturbance locations in the system. The poles of the closed-loop transfer function are the roots of the denominator of Eq. (11):

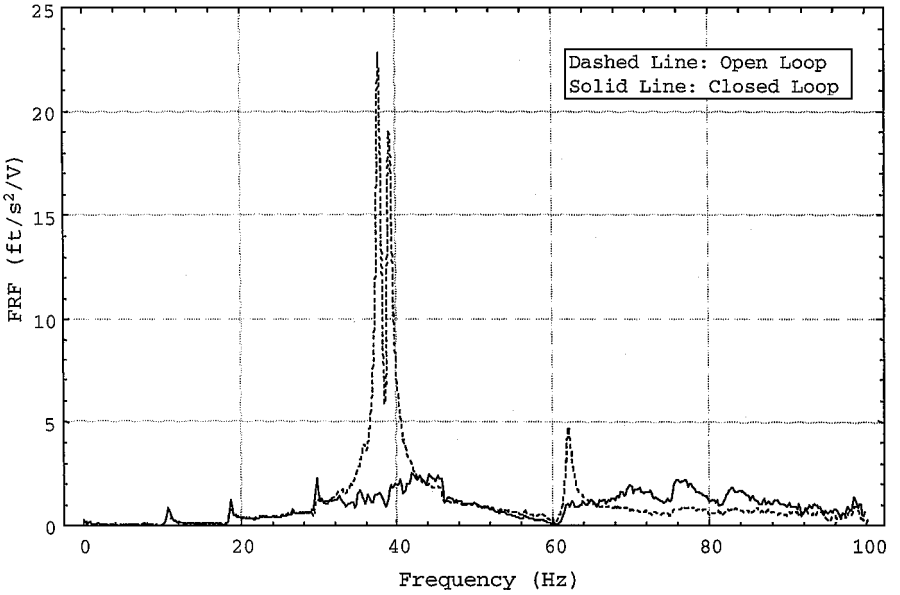


**Fig. 6 Comparison of experimental open- and closed-loop transfer functions.**

$$\text{den}\left(\left.\frac{\bar{y}_p}{\bar{f}_k}\right|_{cl}\right) = \text{den}\left[G_{pk} + \sum_i G_{ci}(G_{pui}G_{sk} - G_{sui}G_{pk})\right] \times \text{num}\left(1 - \sum_i G_{ci}G_{sui}\right) \tag{12}$$

It can be shown that the first term of the left-hand side of Eq. (12) does not depend on the performance sensor location. Hence, the equation can be simplified by collocating the performance and control sensors. The characteristic equation is then given by

$$0 = \text{den}(G_{sk}) \times \text{num}\left(1 - \sum_i G_{ci}G_{sui}\right) \tag{13}$$

Equation (13) is also independent on the disturbance excitation location, so that we finally obtain, using the $k$th actuator array for disturbance,

$$0 = \text{den}(G_{suk}) \times \left\{\prod_i \text{den}(G_{ci}G_{sui}) - \sum_i \left[\text{num}(G_{ci}G_{sui}) \prod_{j \neq i} \text{den}(G_{cj}G_{suj})\right]\right\} \tag{14}$$

The closed-loop stability is assessed by computing the roots of Eq. (14), before implementing the controllers.

## Validation on Laboratory Vertical Tail Subassembly

The usefulness of the combination of acceleration feedback control and piezostack actuator assembly for multimode control was validated by controlling the vibrations of the full-scale vertical tail subassembly of the HPTTA shown in Fig. 2. For this experiment, the sensor was located on the inboard trailing-edge tip of the vertical tail so that it had a maximum sensing of bending and torsion modes. The piezostack actuator assembly was mounted on the inboard side of the tail, at two-thirds, of its span, on the leading-edge side of the elastic axis.

The design of the vertical tail vibration controller using an AFC scheme was set up such that it would increase the damping of three modes, that is, all significant modes between 20 and 80 Hz, using a single actuator array. The three modes that were chosen were the first torsion mode, a plate mode with a diagonal node line, and the second bending mode of the vertical tail. Each of the compensators is designed independently. The type of single-degree-of-freedom AFC chosen was the crossover design for all three modes.

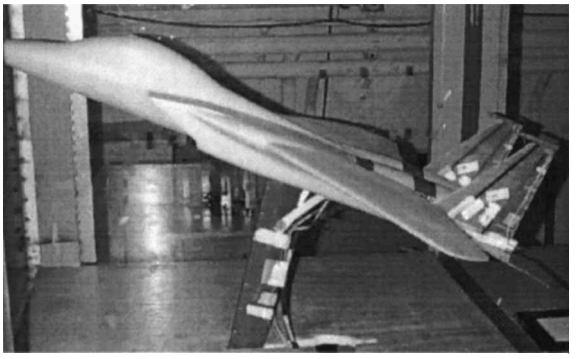

**Fig. 7 HPTTA $\frac{1}{16}$th-scale model mounted in the wind tunnel.**

The compensator parameters are computed with an initial choice of compensator damping ratio of about 10 times the modal-damping coefficient of the associated mode of the open-loop structure. The results, shown in Fig. 6, demonstrate the ability of acceleration feedback control to reduce the vibration amplitude of multiple modes using a single array of piezostack actuator assemblies.

## Wind-Tunnel Tests to Design Actuator Parameters

A $\frac{1}{16}$th-scale wind-tunnel model, shown in Fig. 7, was designed and built. This model consisted of a rigid fuselage and wings with an aeroelastically scaled empennage. To determine the needed control authority and to obtain information to design OPSA parameters, two arrays of piezoceramic wafers were bonded on both of the scaled vertical tails. For each tail, the first array was located at its root to control the bending modes. This array was made of two pairs of piezoceramic wafers in a bender configuration. The second array was optimized to control the torsion modes and was located above the first array. An accelerometer was mounted on the inboard trailing edge of the tip of each vertical tail. The configuration of the wind-tunnel model is shown in Fig. 8.

Wind tunnel tests were performed at the Georgia Tech Research Institute Model Test Facility (GTRI-MTF). The GTRI-MTF wind tunnel is a closed-return, atmospheric, low-speed wind tunnel that has a rectangular test section 76.30 cm (30 in.) high and 109.22 cm (43 in.) wide with a usable length of 228.60 cm (90 in.). This facility is capable of empty tunnel speeds up to 60.96 m/s (200 ft/s) and corrected maximum dynamic pressures of 2.394 kPa (50 psf). During the tests, wall corrections were not considered for the following reasons. The vortices, which are responsible for the buffet, are formed near the junction of the fuselage, the engine inlets, and wing leading edges. Furthermore, the tail subassembly, where the measurement

of buffet loads are obtained, is near the center of the tunnel cross section. Because blockage correction factors for separated flow were not available, the freestream dynamic pressure was corrected by using approximate correction factors that were obtained from flows at low angles of attack.

To determine the modes that should be controlled on the $\frac{1}{16}$th-scale model, a wind-tunnel experiment was designed. This experiment was performed with the wind-tunnel dynamic pressure set at $q = 335.16$ Pa (7 psf), and the scale model was mounted at an angle of attack $\alpha = 22$ deg. The results of this experiment demonstrated that modes with frequencies between 25 and 90 Hz were dominant, as shown in Fig. 9. These correspond to the first torsion mode, a plate mode with a diagonal node line, and the second bending mode.

It was decided to control only the left vertical tail. The first and fourth modes were controlled using the actuator array at the root. The second and third modes were controlled using the upper wafer pair.

First, the transfer function between the lower array and the accelerometer mounted on the inboard trailing-edge tip of the vertical tail was determined. Then, a controller was designed with two compensators in parallel. Each compensator followed the theory of AFC with a crossover-point-based designed.[21] Once this controller was designed, it was validated with zero airspeed. Then, a second transfer function was obtained by vibrating the vertical tail using the upper actuator pair while controlling the first and fourth modes with the lower wafers. This transfer function was taken between the upper piezoceramic actuators and the accelerometer sensor. Also using AFC with crossover conditions, a controller was designed to damp the vibrations of the second and third modes. Then, both controllers were implemented simultaneously with zero airspeed.

The result of the wind-tunnel tests for a dynamic pressure of $q = 335.16$ Pa (7 psf) is shown in Fig. 10. For this experiment, the model was mounted at a 22-deg angle of attack. All four controlled modes were reduced only by a factor close to 2 and not 5. Even for this factor of 2 and $q = 335.16$ Pa (7 psf), maximum voltage at the input of the piezodriver was attained, more than once, during the experiment. This information was used to scale the parameters and design the piezoceramic stack-based actuator assemblies that can reduce the vibration magnitude at least by a factor of 5 and $q = 430.92$ Pa (9 psf) to simulate approximately the flight conditions of the buffet in the selected HPTTA.

**Fig. 8 Instrumented vertical tails mounted on the scale model.**

## Tests for Active Tail Buffet Alleviation

Experiments reported by Triplett[35] and Komerath et al.[3] showed that there exists a characteristic frequency associated with the maximum buffet load and that its associated reduced frequency is almost the same for all experiments. Hence, the models selected for the tail buffet alleviation tests were scaled such that the reduced frequencies are conserved. To operate in the middle of the optimal range for the GTRI-MTF wind tunnel, the scale model of the empennage had the natural frequencies 2.25 time larger than the natural frequencies of the full-scale tail subassembly. This model would then operate at a freestream dvnamic pressure of 430.92 Pa (9 psf) to conserve the reduced frequencies of the flow and structure. This dynamic pressure was equivalent to a freestream velocity of 26.9 m/s (88.25 ft/s) and very approximately simulated the flight buffet conditions.

Buffet load and dynamic response measurements were taken. The results of this experiment showed that the frequency associated with the maximum buffet load evolves linearly with freestream velocity, which confirmed that the reduced frequency associated with the maximum buffet load remains constant. Then, a flow visualization experiment involving tufts attached to the model was performed. This test showed that (seen from the rear) a clockwise vortex immersed the left vertical tail with its core outboard of it. To maintain the vortex cohesion and a minimum flow disturbance due to the sensor, the optimum location for the sensor was on the trailing-edge tip of the vertical tail. The placement was verified experimentally. All modes in the control range were observable.

The next phase was to determine the angle of attack for the worst buffet-induced loads on the vertical tail. The dynamic response of the vertical tail was measured instead of the pressure. A survey was conducted for angles of attack ranging from 0 to 23 deg, which showed that the angle of attack that displays the maximum tip response

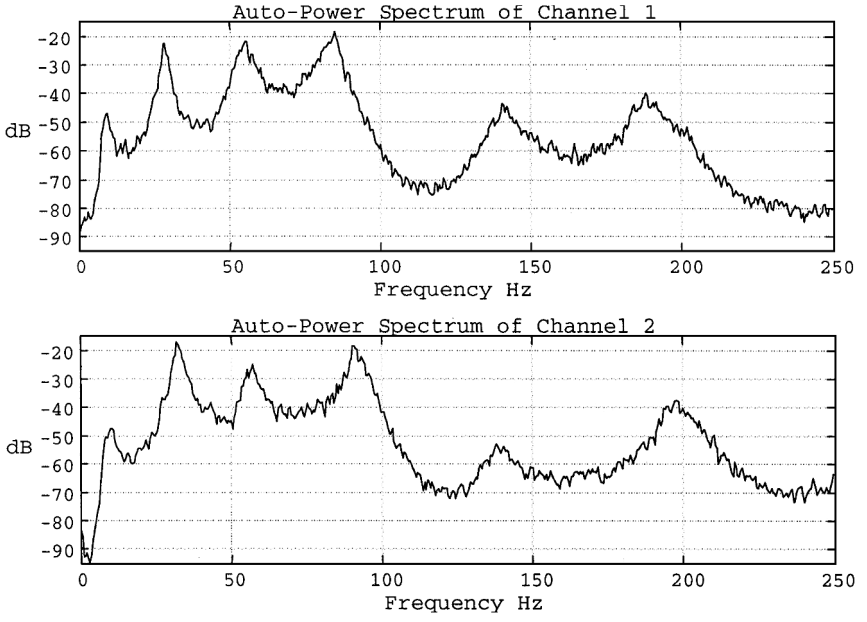


**Fig. 9 Autopower spectrums of the left vertical tail (channel 1) and right vertical tail (channel 2) at $q$ = 335.16 Pa (7 psf) and $\alpha$ = 22 deg.**

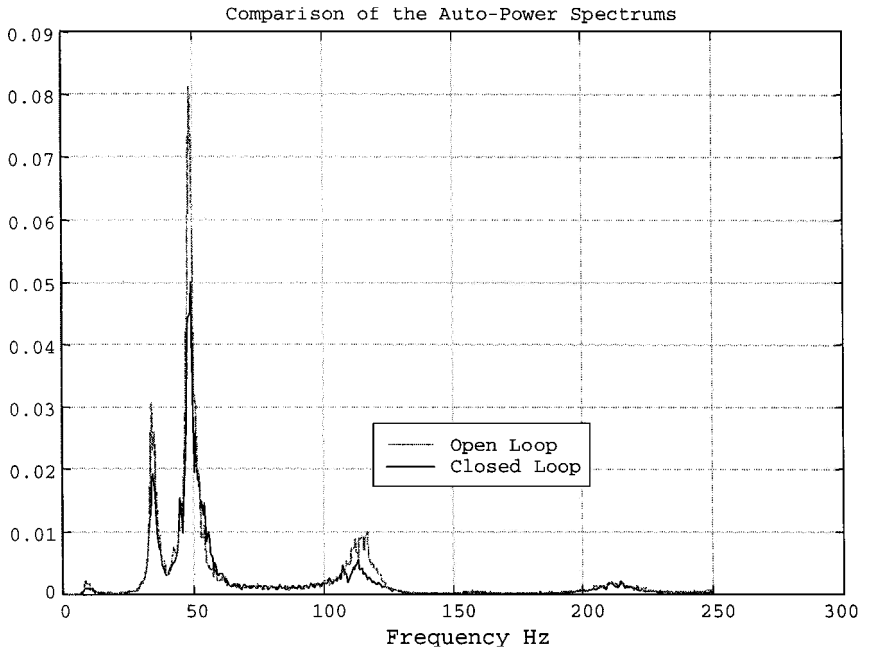


**Fig. 10 Comparison of open-loop and closed-loop autopower spectrum of the acceleration of the tip of the vertical tail.**

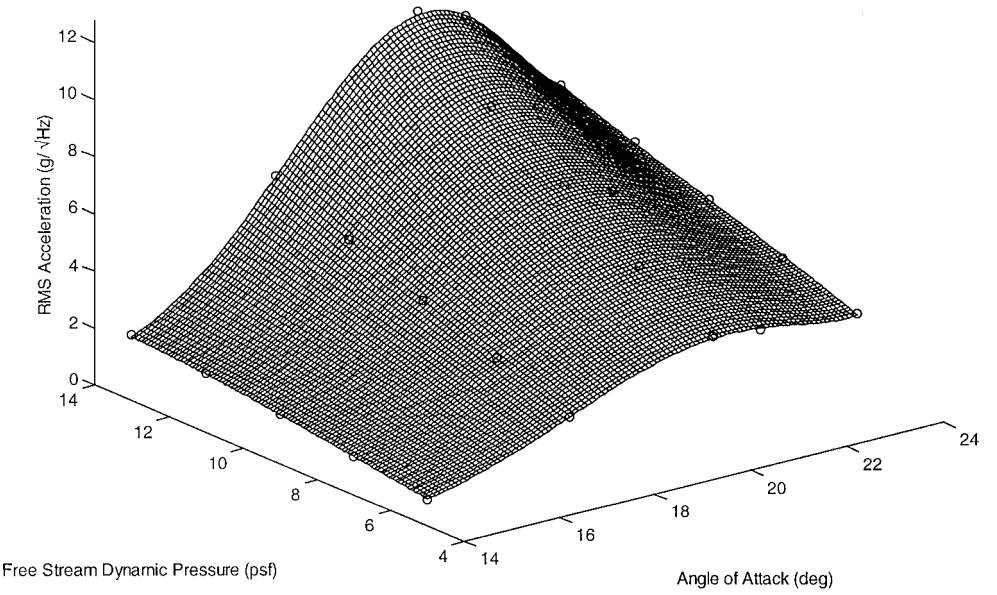


**Fig. 11 Envelope of root mean square of the trailing-edge tip acceleration vs angle of attack and freestream dynamic pressure.**

was approximately 20 deg. This critical angle of attack provides the worst condition on the basis of the geometric conditions between the vortices and the fin. The speed, however, determines the magnitudes of the excitation of the fin modes. To determine this condition, a second survey was conducted for different angles of attack and freestream dynamic pressures in the neighborhood of 20 deg to obtain the buffet dynamic response envelope shown in Fig. 11.

At this point, the left vertical tail was instrumented with two pairs of piezoceramic-stack-based actuators. The first pair of actuators was located to obtain large bending actuation authority and was bonded at the root of the vertical tail along its midchord line. The second pair of piezoceramic stack actuators was placed for torsion control and was bonded at 35 deg with respect to the midchord line above the first pair. This configuration is shown in Fig. 12. To refine the plant model, experimental transfer functions were obtained between the input voltage to each actuator array and the sensor response voltage. Then, when system identification techniques were used, transfer functions were extracted. To experimentally assess the authority of the actuator arrays, the autopower spectrum of the

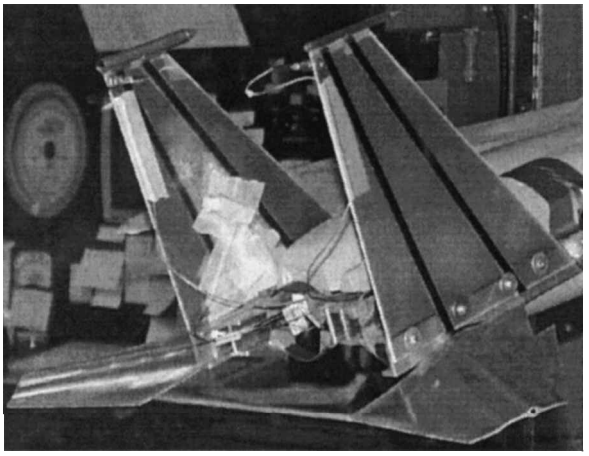

**Fig. 12 Active buffet alleviation experiment vertical tails with piezostack actuators.**

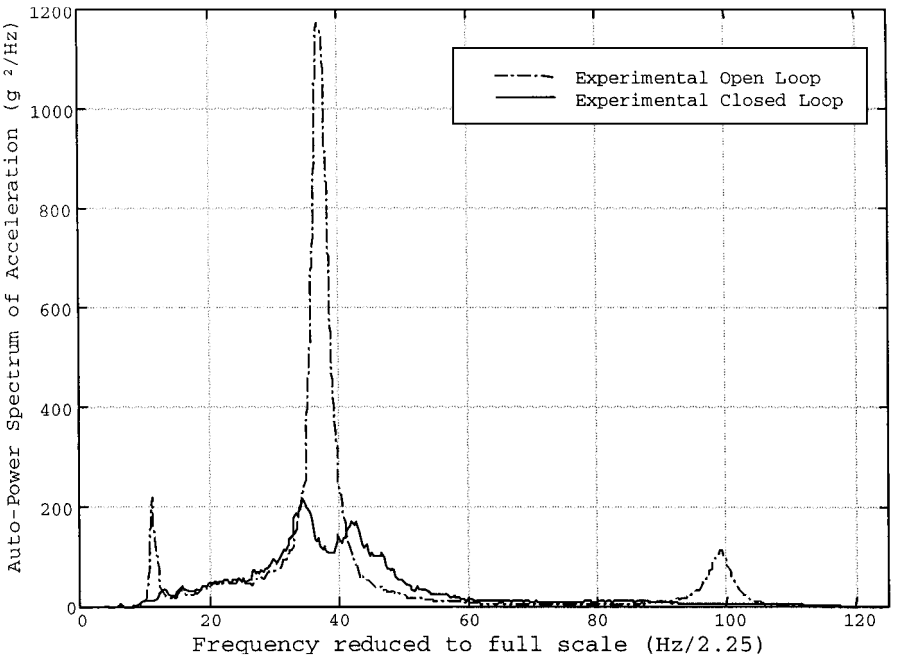


**Fig. 13 Comparison between open- and closed-loop autopower spectrum of trailing-edge tip acceleration at $\alpha$ = 20 deg and $q_\infty$ = 430.92 Pa (9 psf).**

dynamic response of the sensor, excited by the buffet vortices, was compared with the autopower spectra of the actuator arrays. Power spectra were obtained, from the experimental transfer functions of the plant, for a flat maximum input voltage. This operation showed that enough actuator authority was attained.

Once the plant model had been developed and the actuator authority checked, the AFC controller parameters were obtained. Results of the earlier tests indicated that the crossover point design did not always result in a single closed-loop frequency for multimode control. In addition, the crossover point design was not always as robust as the controller with $H_2$ optimization. Thus, the type of AFC design selected was the $H_2$ optimization of the closed-loop transfer function (Ref. 34 and Bayon de Noyer and Hanagud, to be published). Two different controllers were designed, one for the bending array and one for the torsion array. A single-degree-of-freedom compensator was designed for each mode using the parameters extracted earlier. To avoid clipping of the control signals, the damping of each compensator was limited to be seven times larger than the damping of the associated mode. Once the controllers were designed, their stability and effects on other modes were checked using root locus plots. Root locus plots did not show any instability, and each controller did not affect the parameters of the other controller. This confirmed our hypothesis to use a combination of single-degree-of-freedom design of controllers and to implement both the controllers simultaneously.

The controllers were implemented by using a digital signal processor (DSP) DS1003 that was manufactured by dSPACE Corporation. The needed programming for the control experiment was done using commercially available software MATLAB®, MATLAB extension Simulink, and Trace. The program file was then converted to the machine language of the DSP and downloaded to the DSP system. Once the system started, the controllers were active.

To validate the controllers, three different experiments were performed. First, a control experiment was run at the predetermined operating condition of 20-deg angle of attack and 430.92 Pa (9 psf) of freestream dynamic pressure. The autopower spectra of the uncontrolled and controlled trailing-edge tip acceleration are shown in Fig. 13. As seen in Fig. 13, the magnitude of the autopower spectrum, at each of the controlled frequencies, is reduced by a factor of at least 5. Furthermore, in the case of the first bending mode and second torsion mode, the responses are suppressed to a level equivalent to the one that would be obtained in the absence of these modes. At frequencies that are significantly away from the frequencies corresponding to the maximum dynamic loads, the attenuation is small but the absolute magnitudes of the response are very small. This is because the design of the AFC was targeted to reduce the maximum loads at the selected frequencies.

Once the controller had been validated at its operating point (angle of attack of 20 deg), its effectiveness is checked at different conditions in the second set of experiments. For the second experiment, the operating freestream dynamic pressure of 430.92 Pa (9 psf) was kept. However, the angle of attack was varied from 0 to 23 deg. This control experiment showed that the root mean square of the trailing-edge tip acceleration was reduced by up to 30% below 15 deg and by about 20% at 20 deg. This experiment also showed that the controllers were effective on the whole range of angles of attack.

Finally, in the third set of experiments, four different angles of attack were selected; 14, 17, 20, and 23 deg were chosen to cover the different regimes of buffet that the scaled model can encounter. For each angle of attack, the freestream dynamic pressure was varied from 239.40 to 622.44 Pa (5 to 13 psf). As before, the results showed that as the disturbance increases the effectiveness of the controller decreases. However, even at a freestream velocity 25% higher than the operating freestream velocity, the minimum rms reduction was still 17%. These results prove that the controllers were stable and effective over the full buffet domain, which means angles of attack ranging from 14 to 23 deg and freestream velocity ranging from $-25$ to $+25\%$.

## Conclusions

In this paper, we have clearly shown that the tail buffet-induced vibrations can be controlled using smart structure concepts. The theoretical and experimental investigations have shown that it is possible to obtain the required control authority for tail buffet alleviation by using piezoceramic-stack-based actuators. This was accomplished 1) by designing an effective actuator assembly, 2) by developing procedures to place optimally the sensors and actuators on the vertical tail subassembly, 3) by designing controllers using acceleration feedback control concepts, and 4) by developing procedures to implement these controllers using DSP-based systems and specially written algorithms. The effectiveness of multimode controllers was validated by 1) testing the full-scale laboratory subassembly under excitation provided by a shaker and 2) wind-tunnel tests on a $\frac{1}{16}$th-scale model with aeroelastically tailored vertical tail subassembly.

## Acknowledgments

The authors gratefully acknowledge the support of the U.S. Air Force under the Small Business Innovation Research Program,

Contract F33615-96-C-3204 and the associated subcontract to Georgia Tech. The authors also acknowledge the Georgia Institute of Technology for support of the in-house research program. The authors would like to acknowledge the technical support of Robert J. Englar and Robert B. Funk from the Georgia Tech Research Institute during the wind-tunnel tests.

## References

[1]Ferman, M. A., Liguore, S. L., Smith, C. M., and Colvin, B. J., "Composite Exoskin Doubler Extends F-15 Vertical Tail Fatigue Life," *Proceedings of the 34th Structures, Structural Dynamics, and Materials Conference*, Vol. 1, AIAA, Washington, DC, 1993, pp. 398–407.

[2]Wentz, W. H., and Kohlman, D. L., "Vortex–Fin Interaction of a Fighter Aircraft," AIAA Paper 87-2474, 1987.

[3]Komerath, N. M., Schwartz, R. J., and Kim, J. M., "Flow over a Twin-Tailed Aircraft at Angle of Attack, Part II: Temporal Characteristics," *Journal of Aircraft*, Vol. 29, No. 4, 1992, pp. 553–558.

[4]Bean, D. E., Greenwell, D. I., and Wood, N. J., "Vortex Control Technique for the Attenuation of Fin Buffet," *Journal of Aircraft*, Vol. 30, No. 6, 1993, pp. 847–853.

[5]Bean, D. E., and Wood, N. J., "Experimental Investigation of Twin-Fin Buffeting and Suppression," *Journal of Aircraft*, Vol. 33, No. 4, 1996, pp. 761–767.

[6]Hebbar, S. K., Platzer, M. F., and Frink, W. D., "Effect of Leading-Edge Extension Fences on the Vortex Wake of an F/A-18 Model," *Journal of Aircraft*, Vol. 32, No. 3, 1995, pp. 680–682.

[7]Meyn, L. A., and James, K. D., "Full-Scale Wind-Tunnel Studies of F/A-18 Tail Buffet," *Journal of Aircraft*, Vol. 33, No. 3, 1996, pp. 589–595.

[8]Pettit, C. L., Brown, D. L., Banford, M. P., and Pendleton, E., "Full-Scale Wind-Tunnel Pressure Measurements of an F/A-18 Tail During Buffet," *Journal of Aircraft*, Vol. 33, No. 6, 1996, pp. 1148–1156.

[9]Gee, K., Murman, S. M., and Schiff, L. B., "Computation of F/A-18 Tail Buffet," *Journal of Aircraft*, Vol. 33, No. 6, 1996, pp. 1181–1189.

[10]Klein, M. A., and Komerath, N. M., "Reduction of Narrow-Band Velocity Fluctuation over an Aircraft Model," AIAA Paper 97-2266, 1997.

[11]Ferman, M. M., and Turner, E. W., "An Experimental Investigation of Tangential Blowing to Reduce Buffet Response of the Vertical Tails of an F-15 Wind Tunnel Model, Vol. I—Test Result, Discussion, and Correction," U.S. Air Force Research Lab., Rept. AFRL-VA-WP-1999-3018, Wright–Patterson AFB, OH, Jan. 1999.

[12]Ferman, M. M., and Turner, E. W., "An Experimental Investigation of Tangential Blowing to Reduce Buffet Response of the Vertical Tails of an F-15 Wind Tunnel Model, Vol. II—Detailed Data Test—Flexible Model Response," U.S. Air Force Research Lab., Rept. AFRL-VA-WP-1999-3019, Wright–Patterson AFB, OH, Jan. 1999.

[13]Ferman, M. M., and Turner, E. W., "An Experimental Investigation of Tangential Blowing to Reduce Buffet Response of the Vertical Tails of an F-15 Wind Tunnel Model, Vol. III—Oscillatory Pressure Data," U.S. Air Force Research Lab., Rept. AFRL-VA-WP-1999-3020, Wright–Patterson AFB, OH, Jan. 1999.

[14]Huttsell, L. J., Tinapple, J. A., Weyer, R. M., "Investigation of Buffet Load Alleviation on a Scaled Twin Tail Model," AGARD Rept. R-822, Oct. 1997.

[15]Zimmerman, N. H., and Ferman, M. A., "Prediction of Tail Buffet Loads for Design Applications," U.S. Navy Rept., NADC-88043-60, July 1997.

[16]Zimmerman, N. H., Ferman, M. A., Yurkovich, R. N., and Gersternkorn, G., "Prediction of Tail Buffet Loads for Design Applications," *Proceedings of the AIAA/ASME/ASCE/AHS/ASC 30th Structures, Structural Dynamics, and Materials Conference*, AIAA, Washington, DC, 1989, pp. 1911–1919.

[17]Ferman, M. A., Patel, S., Zimmerman, N. H., and Gersternkorn, G., "A Unified Approach to Buffet Response of Fighter Aircraft Empennage," CP-483, AGARD, Sept. 1990, pp. 2.1–2.18.

[18]Ferman, M. A., and Liguore, S. L., "Buffet Coupled Response of the HARV Thrust Vectoring Vane System," NASA High-Angle-of-Attack Conf., Hampton, VA, Oct. 1990.

[19]Washburn, A. E., Jenkins, L. N., and Ferman, M. A., "Experimental Investigation of Vortex-Fin Interaction," AIAA Paper 93-0050, April 1993.

[20]Fermna, M. A., Liguore, S. L., Colvin, B. L., and Smith, S. M., "Composite Exoskin Doubler Extends F-15 Vertical Tail Fatigue Life," AIAA Paper 93-1341, April 1993.

[21]Dima, C., "The Effects of Time Varying Maneuver Conditions on Empennage Buffet Response," M.S. Thesis, Aerospace and Mechanical Engineering, Parks College, St. Louis Univ., St. Louis, MO, Dec. 1994.

[22]Ashley, H., Rock, S. M., Digumarthi, R., Channey, K., and Eggers, A. J., "Active Control for Fin Buffet Alleviation," Flight Dynamic Directorate, Wright Lab., Air Force Material Command, Rept. WL-TR-93-3099, Wright–Patterson AFB, OH, 1994.

[23]Nitzsche, F., Zimcik, D. G., and Langille, K., "Active Control of Vertical Fin Buffeting with Aerodynamic Control Surface and Strain Actuation," *Proceedings of the 38th Structures, Structural Dynamics, and Materials Conference*, Vol. 2, AIAA, Reston, VA, 1997, pp. 1467–1477.

[24]Moses, R. W., "Vertical-Tail-Buffeting Alleviation Using Piezoelectric Actuators: Some Results of the Actively Controlled Response of Buffet-Affected Tails (ACROBAT) Program," *Proceedings of the Society of Photo-Optical Instrumentation Engineers*, Vol. 3044, Society of Photo-Optical Instrumentation Engineers, Bellingham, WA, 1997, pp. 87–98.

[25]Lazarus, K. B., Saarmaa, E., and Agnes, G. S., "Active Smart Material System for Buffet Load Alleviation," *Proceedings of SPIE Smart Structures and Materials: Industrial and Commerical Applications of Smart Structures Technologies*, Vol. 2447, Society of Photo-Optical Instrumentation Engineers, Bellingham, WA, 1995, pp. 179–192.

[26]Hauch, R. M., Jacobs, J. H., Ravindra, K., and Dima, C., "Reduction of Vertical Tail Buffet Response Using Active Control," *Journal of Aircraft*, Vol. 33, No. 3, 1996, pp. 617–622.

[27]Moore, J. W., Spangler, R. L., Lazarus, K. B., and Henderson, D. A., "Buffet Load Alleviation Using Distributed Piezoelectric Actuators," *Industrial and Commercial Applications of Smart Structures Technologies*, Aerospace Div. Vol. 52, American Society of Mechanical Engineers, Fairfield, NJ, 1996, pp. 485–490.

[28]Luo, H., and Hanagud, S., "PVDF Sensor and Its Applications in Curvature Mode Based Damage Detection," *Journal of Aerospace Engineering*, Vol. 12, No. 1, 1999, pp. 23–30.

[29]Goh, C. J., and Caughey, T. K., "On the Stability Problem Caused by Finite Actuator Dynamics in the Collocated Control of Large Space Structures," *International Journal of Control*, Vol. 41, No. 3, 1985, pp. 787–802.

[30]Juang, J. N., and Phan, M., "Robust Controller Designs for Second-Order Dynamic Systems: A Virtual Passive Approach," *Journal of Guidance, Control, and Dynamics*, Vol. 15, No. 5, 1992, pp. 1192–1198.

[31]Sim, E., and Lee, S. W., "Active Vibration Control of Flexible Structures with Acceleration Feedback," *Journal of Guidance, Control, and Dynamics*, Vol. 16, No. 2, 1993, pp. 413–415.

[32]Goh, C. J., and Yan, W. Y., "Approximate Pole Placement for Acceleration Feedback Control of Flexible Structures," *Journal of Guidance, Control, and Dynamics*, Vol. 19, No. 1, 1996, pp. 256–259.

[33]Bayon de Noyer, M., and Hanagud, S., "Single Actuator and Multi-Mode Acceleration Feedback Control," *Adaptive Structures and Material Systems*, Aerospace Div. Vol. 54, American Society of Mechanical Engineers, Fairfield, NJ, 1997, pp. 227–235.

[34]Bayon de Noyer, M., and Hanagud, S., "A Comparison of $H_2$ Optimized Design and Cross-Over Point Design for Acceleration Feedback Control," AIAA Paper 98-2091, 1998.

[35]Triplett, W. E., "Pressure Measurements on Twin Vertical Tails in Buffeting Flow," *Journal of Aircraft*, Vol. 20, No. 11, 1983, pp. 920–925.

E. Livne
*Associate Editor*